Inorg. Chem. **2003**, *42*, 8748–8754

$SrSn_4$: A Superconducting Stannide with Localized and Delocalized Bond Character

Stefan Hoffmann and Thomas F. Fässler*

Eduard-Zintl Institute of Inorganic and Physical Chemistry, Technical University of Darmstadt, Petersenstrasse 18, D-64287 Darmstadt, Germany

Received June 26, 2003

The title compound is the tin-richest phase in the system Sr–Sn and is obtained by stoichiometric combination of the elements. $SrSn_4$ peritectically decomposes under formation of $SrSn_3$ and Sn at 340 °C. The structure determined from a single crystal shows a new structure type with a novel structure motive in tin chemistry. It can be described by a corrugated, distorted quadratic net of tin atoms as the only building unit. The nets intersect at common Sn atoms, and the resulting channels host the Sr atoms. The structure can alternatively be described as an intergrowth structure of the AlB_2-type and W-type. The atoms that are connected by the two shortest Sn–Sn distances (2.900 and 3.044 Å) form a two-dimensional net consisting of hexagons of tin atoms. The hexagons have boat conformation in contrast to the rather similar α-As structure type, where hexagons have a chair conformation. Further tin atoms connect the two-dimensional net of Sn hexagons. Temperature-dependent magnetic susceptibility measurements show that $SrSn_4$ is superconducting with $T_c = 4.8$ K at 10 G. LMTO band structure and density of states calculations verify the metallic behavior of $SrSn_4$. An analysis of the electronic structure with the help of the electron localization function (ELF) shows that localized covalent bonds beside delocalized bonds coexist in $SrSn_4$.

Introduction

One of the most prominent candidates to study the relationship between atomic structure and physical properties is the element tin, since tin has the outstanding property that there exist a metallic and nonmetallic allotrope almost equal in stability. The difference of the thermodynamically more stable α form compared to the β form is only 2 kJ mol^{-1}. This fact manifests also in binary phases of tin and electropositive metals. On the tin-rich side compounds form structures that are typical for intermetallic compounds, but there exist also examples which form structures that are typical for valence compounds and furthermore compounds that are intermediate between the two classes and which possess both structural motives.[1−3]

Several binary phases of tin and alkaline earth metals (AE) are known: The AESn phases for AE = Ca to Ba crystallizes with CrB structure type. The structure contains linear zigzag chains $^1_\infty[Sn^{2-}]$.[4] Exclusively two-fold bonded Sn atoms are expected from the $8 - N$ rule; thus, the compounds fulfil the valence rules. In these so-called Zintl phases all valence electrons are assigned to the tin atoms and the electrons are localized in either two-center−two-electron (2c−2e) bonds between these atoms (tin−tin separation of 2.9 Å) or in form of lone pairs at the tin atoms. At higher tin content A_3Sn_5 phases are known for AE = Sr and Ba. The tin atoms form five-atom clusters with weak interactions between them (shortest intercluster tin−tin contacts are 3.397 and 3.694 Å for AE = Sr and Ba, respectively). In this case the Zintl concept can be extended by the introduction of the electron-counting scheme according to Wade rules. Electron transfer from the AE atoms to tin leads to the polyanion $[Sn_5]^{6-}$, which indeed has an arachno-type structure and derives from a pentagonal bipyramid by removing two adjacent cluster vertexes.[5] However, band structure calculations show that these compounds are metallic. At higher tin content the binary phases $SrSn_3$,[6] $BaSn_3$,[7] and $BaSn_5$[8] are structurally characterized. They are metallic and even superconducting

* To whom correspondence should be addressed. E-mail: faessler@ac.chemie.tu-darmstadt.de. Fax: 0049-6151-166029.

(1) Schäfer, H.; Eisenmann, B.; Müller, W. *Angew. Chem., Int. Ed. Engl.* **1997**, *36*, 2683; **1973**, *85*, 742−760.
(2) Corbett, J. D. In *Chemistry, Structure, and Bonding of Zintl Phases and Ions*; Kauzlarich, S. M., Ed.; VCH Publishers: Weinheim, Germany, 1996; p 139.
(3) Fässler, T. F.; Hoffmann, S. *Z. Kristallogr.* **1999**, *11*, 722−734.
(4) Eckerlin, P.; Meyer, H. J.; Wölfel, E. *Z. Anorg. Allg. Chem.* **1955**, *307*, 145.
(5) Zürcher, F.; Nesper, R.; Hoffmann, S.; Fässler, T. F. *Z. Anorg. Allg. Chem.* **2001**, *627*, 2211−2219.

10.1021/ic0302128 CCC: $25.00 © 2003 American Chemical Society
Published on Web 11/22/2003

at temperatures below 5.4 K ($SrSn_3$), 2.4 K ($BaSn_3$), and 4.4 K ($BaSn_5$). $SrSn_3$ and $BaSn_3$ can be regarded as compounds at the borderline of structures, which derive from closest packing of spheres and Zintl phases with localized chemical bonds. The structures can be described as distorted hexagonal or cubic closest atom packing as it is known for a variety of intermetallic compounds of the composition $M'M_3$. However, formal electron transfer from AE to tin atoms leads to the formula $[Sn_3]^{2-}$ and gets another perspective on the structure. The closest packing contains trimember rings of tin atoms, and the structures can be broken down to the polyanionic Zintl-anionic unit $[Sn_3]^{2-}$ with an aromatic 2π-electron system. Interactions between these units through their π-electron systems are strong, and almost equal intra- and inter-ring contacts are observed. Finally, in the tin-richest phase $BaSn_5$ tin atoms form graphite-like layers (honeycombs). Two such layers built a slab of hexagonal prisms, which are centered by additional Sn atoms. The central tin atom has 12 nearest neighbors of tin atoms and represents the first case of a tin atom with such high coordination number. The slabs are separated by Ba atoms above and below the center of each tin hexagon.[8]

During our systematic investigation of the Sr/Sn phase system we were now able to determine the structure and the physical properties of the tin-richest phase in the Sr−Sn system $SrSn_4$.

Experimental Section

Synthesis. $SrSn_4$ was synthesized as a pure phase via combination of the elements. Stoichiometric amounts of strontium (ALFA 99.9%, distillation prior to use) and tin (Aldrich, 99.5%) were heated in a sealed niobium ampule at 200 °C/h to 900 °C. The sample were held at this temperature for 3 h, quenched to room temperature, and annealed at 315 °C for 22 days. The X-ray diffraction diagram of a powdered sample shows the presence of $SrSn_4$ as single phase.

The DTA of the product indicates the presence of small amount of the eutectic of Sn−$SrSn_4$ (endothermic effect at 220 °C). Furthermore an endothermic effect with a T_{onset} = 340 °C is observed. According to Marshall et al. this effect corresponds to the decomposition of $SrSn_4$.[9] The complete melting of the sample is accompanied by a broad effect in the range between 500−600 °C. On cooling the reversed processes are observed and the powder diffraction diagram of the product after the DTA experiment shows lines of $SrSn_3$,[6] $SrSn_4$, and Sn.

X-ray Structure Determination. Single crystals of $SrSn_4$ for diffraction studies were selected from the reaction of Sr and Sn in the ratio 1:8. A sealed niobium ampule was heated at 150 °C/h to 500 °C, held there for 20 h, and cooled to room temperature at the same rate. The product was annealed over 2 months in a sealed steel ampule at 320 °C. The ingot was ductile and contains cuboid crystals of $SrSn_4$. Crystals were mounted in glass capillaries under the microscope in a drybox. Diffraction data were collected on a Siemens SMART system with Mo Kα radiation and a CCD detector. The structures were solved by direct methods (SHELXS-86) and difference Fourier analysis and refined using least-squares cycles based on F^2 (SHELXTL). Further details are listed in Table 3.

Table 1. Atomic Coordinates ($\times 10^4$) and Equivalent Isotropic Displacement Parameters ($Å^2 \times 10^3$) for $SrSn_4$

atom	site	x	y	z	U_{eq}
Sn(1)	8f	0	1959(1)	447(1)	16(1)
Sn(2)	4c	0	5902(1)	1/4	17(1)
Sn(3)	4a	0	0	0	19(1)
Sr(1)	4c	0	3882(1)	1/4	14(1)

Magnetic Measurements. Magnetic susceptibility measurements were performed using a SQUID magnetometer (Quantum Design MPMS 5S). Suprasil quartz capillaries (5 mm diameter) served as sample holders. The sample was cooled in the absence of a magnetic field checked before by an external Hall probe. After the introduction of a 10 G field, data were recorded while the sample was warmed ("shielding") and then cooled ("Meissner"). The magnetization at different external fields was determined at 1.75 K. The shielding fraction was determined from the slope of the curve in the linear part. The corrections of the magnetic data were made to account for demagnetization effects by assuming a spherical shape for the superconducting particles with demagnetization factor $n = 1/3$.

Electronic Structure Determination. The electronic structure was calculated with the local density-functional approach and the linear muffin-tin orbital (LMTO) method in the atomic sphere approximation (ASA) using the tight-binding (TB) program TB-LMTO-ASA.[10] The exchange correlation potential was parametrized according to Barth and Hedin.[11] The radii of the muffin-tin spheres and empty spheres were determined after Jepsen and Andersen.[12] For the calculation s, p, and "down folded" d-partial waves for Sn and s, d, and "down-folded" p-partial waves for Sr were used.

Results

Structure. The histogram of Sn−Sn distances shows a gap between 3.530 and 4.161 Å. The group of shorter Sn−Sn contacts below 3.530 Å is further divided into three subgroups. Shortest contacts occur between Sn(1) atoms (2.90 and 3.04 Å) and are in the range of atom−atom separations of elemental α-Sn (2.81 Å) and β-Sn (3.02 and 3.18 Å). Longer contacts of 3.29 Å appear between Sn(2) and Sn(1) or Sn(2) and Sn(3) atoms, and the longest contacts listed in Table 2 are in the range from 3.42 to 3.51 Å. Taking into account all Sn−Sn distances up to 3.3 Å a three-dimensional network of Sn atoms results as shown in Figure 1. The structure can completely be described by a corrugated, distorted quadratic net of tin atoms as the only building unit as shown in Figure 1b. Tin−tin atom separations within the net are in the range from 3.044 to 3.302 Å and occur between all three different types of Sn atoms. The nets lie with their mean planes parallel to the *a* axes of the orthorhombic unit cell. The two perpendicular planes {021} and {04$\bar{2}$} intersect

(6) Fässler, T. F.; Hoffmann, S. *Z. Anorg. Allg. Chem.* **2000**, *626*, 106−112.
(7) Fässler, T. F.; Kronseder, C. *Angew. Chem., Int. Ed. Engl.* **1997**, *36*, 2683. **1997**, *109*, 2800.
(8) Fässler, T. F.; Hoffmann, S.; Kronseder, C. *Z. Anorg. Allg. Chem.* **2001**, *620*, 2486−2492.
(9) Marshall, D.; Chang, Y. A. *J. Less-Common Met.* **1981**, *78*, 139−145.
(10) van Schilfgarde, M.; Paxton, T. A.; Jepsen, O.; Andersen, O. K.; Krier, G. In *Programm TB-LMTO*; Max-Planck-Institut für Festkörperforschung: Stuttgart, Germany, 1994.
(11) Barth, U.; Hedin, L. *J. Phys. Chem.* **1972**, *5*, 1629.
(12) Jepsen, O.; Andersen, O. K. *Z. Phys. B* **1995**, *97*, 35.

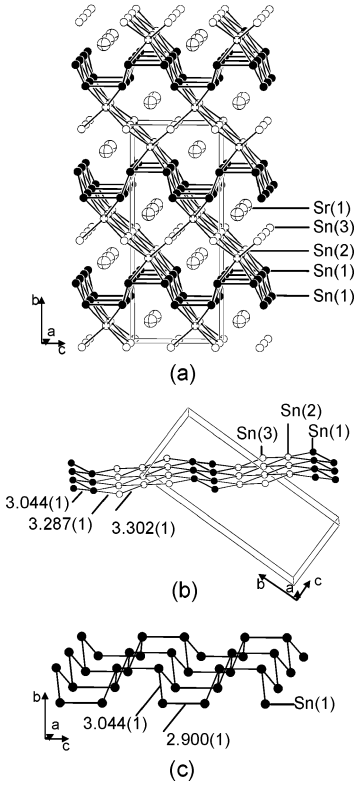

Figure 1. Various details of the crystal structure of $SrSn_4$: (a) all Sn−Sn contacts up to 3.3 Å are shown as solid lines, unit cell outlined; (b) corrugated net of distorted squares of Sn(1), Sn(2), and Sn(3) atoms; (c) net of Sn(1) atoms (all distances in Å; cf. also Table 2).

Table 2. Selected Interatomic Distances in Å with Standard Deviation in Units of the Last Decimal in Parentheses

atom−atom contact	dists	noc	atom−atom contact	dists	noc
Sn(1)− Sn(1)	2.900(1)	1	Sn(3)−Sn(2)	3.302(1)	4
Sn(1)−Sn(1)	3.044(1)	2	Sn(3)−Sn(1)	3.417(1)	2
Sn(1)−Sn(2)	3.287(1)	2	Sn(3)−Sr(1)	3.496(1)	4
Sn(1)−Sn(3)	3.417(1)	1	Sn(3)−Sn(3)	3.530(1)	2
Sn(1)−Sr(1)	3.434(1)	2			
Sn(1)−Sr(1)	3.642(1)	1			
further contacts	≥4.161(1)		further contacts	≥4.618(1)	
Sn(2)−Sn(1)	3.287(1)	4	Sr(1)−Sn(1)	3.434(1)	4
Sn(2)−Sn(3)	3.302(1)	4	Sr(1)−Sn(3)	3.496(1)	4
Sn(2)−Sr(1)	3.510(1)	1	Sr(1)−Sn(2)	3.510(1)	1
Sn(2)−Sr(1)	3.550(1)	2	Sr(1)−Sn(2)	3.550(1)	2
			Sr(1)−Sn(1)	3.642(1)	2
further contacts	≥4.259(1)		further contacts	≥4.618(1)	

Table 3. Data Collection and Refinement Details

empirical formula	$SrSn_4$
fw	562.38
space group, *Z*	*Cmcm*, 4
unit cell params (Å)	$a = 4.6179(9)$, $b = 17.372(4)$, $c = 7.060(1)$
V (Å^3)	566.4(2)
T (K)	293(2)
reflcns collcd	2975
indpndt reflcns	601 ($R_{int} = 0.099$)
R (all data)	$R_1 = 0.044$, $wR_2 = 0.110$
goodness of fit	1.203

at the Sn(2) atoms (Figure 1a). The resulting channels are oriented parallel to the *a* axes and host the Sr atoms. Consequently, the Sr atoms form linear chains with a Sr−Sr atom separation having the length of the *a* axes. Due to the corrugation of the net, short Sn(1)−Sn(1) contacts of 2.900 Å are formed. Alternatively, the structure can be described based on a substructure of Sn atoms, which is

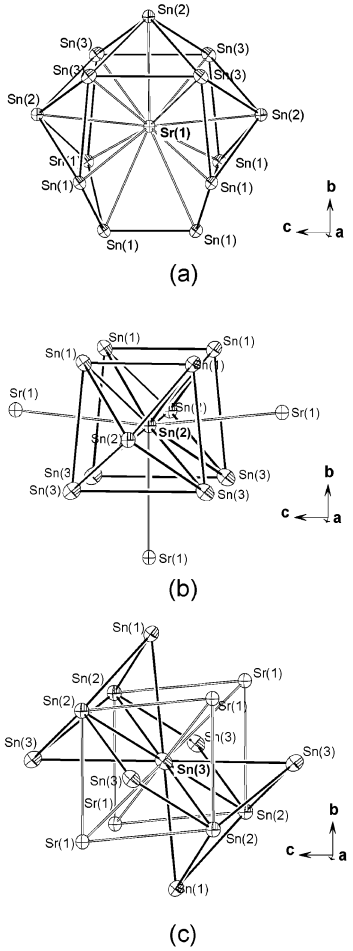

Figure 2. Coordination polyhedra of (a) Sr(1), (b) Sn(2), and (c) Sn(3). Solid lines represent Sn−Sn contacts up to 3.53 Å (for distances see Table 2).

formed by the atoms connected by the two shortest Sn−Sn distances (2.900 and 3.044 Å). Those Sn atoms form a two-dimensional net consisting of six-membered rings of tin atoms. These rings of Sn(1) atoms have a boat conformation (Figure 1c) in contrast to the rather similar α-As structure type, where hexagons take a chair conformation. Sn(2) and Sn(3) atoms connected the two-dimensional net of Sn(1) atoms (Figure 1a).

Further, the structure can be rationalized in terms of rather similar coordination polyhedra of the atoms Sr, Sn(2), and Sn(3). In all cases the structure motive is a distorted quadratic prism. The first coordination sphere of Sr is a distorted quadratic prism of Sn atoms, elongated along the *a* direction (Figure 2a). The distances between the central Sr atom and the corners of the distorted prism are 3.434(1) Å for Sr(1)−Sn(1) and 3.496(1) Å for Sr(1)−Sn(3). Sn−Sn contacts along the edges are longer than 3.530 Å. Three faces along the height of the prism are capped by Sn(2) atoms with a Sn−Sn distance of 3.287 and 3.302 Å; the fourth face is bridged by a dumbbell of Sn(1) atoms at a distance of 3.044 Å. This Sn_2 unit is part of the net of Sn(1) atoms shown in Figure 1c. Interestingly, the atoms Sn(2) and Sn(3) have a rather similar coordination polyhedron (Figure 2b,c, respectively). Sn(2) is surrounded four Sn(1) and four Sn(3) atoms. Sr atoms cap two opposite faces of the distorted quadratic prism

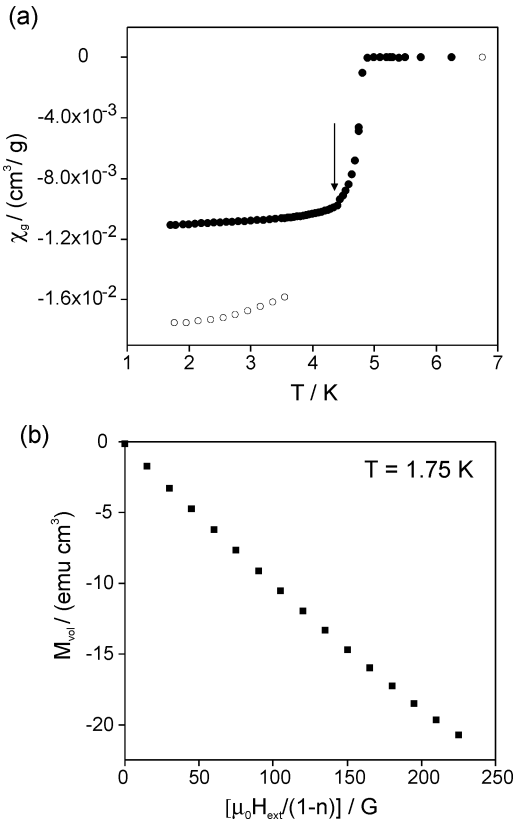

Figure 3. Magnetism of $SrSn_4$ at low temperatures: (a) diamagnetic shielding (○) and Meissner effect (●) at 10 G (the arrow marks a small kink); (b) magnetization at 1.75 K (demagnetization factor $n = 1/3$).

that have mixed atoms sites and the face of Sn(3) atoms. Further capping with Sn(2) atoms is due to translation symmetry along the *a* direction. The coordination polyhedron of Sn(3) is a distorted quadratic prism of Sn(2), and Sr atoms as shown in Figure 2c. The two opposite faces parallel to the *ab* plane are capped with Sn(3) atoms, and two opposite faces parallel to the *ac* plane are capped with Sn(1) atoms. At longer distances two further faces are capped with Sn(3) atoms. The coordination polyhedra are also shown in Figure 6 and will be discussed in more detail below.

Magnetic Properties. The recorded curves for the low-field magnetic susceptibility show the characteristics of a superconductor (Figure 3a). An external field of 10 G applied to a sample, which was cooled in a zero field regime, causes a negative value for the magnetic susceptibility ("shielding"). The pronounced diamagnetic property of $SrSn_4$ vanishes at higher temperatures with the transition temperature of 4.8 K (10 G). During the cooling of the sample in the external field a jump of the susceptibility is observed again, but the value of the shielding curve at the same temperature is not reached (full circles in Figure 3a). This behavior is characteristic for type II superconductors. The large value of the magnetization at 1.75 K shows that the whole sample is in the superconducting state. This was confirmed by measuring the magnetization in dependence of the external field at 1.75 K (Figure 3b). The slope of the linear part gives a shielding fraction of 123% assuming a demagnetization factor of 1/3, which shows that the whole sample and not an impurity

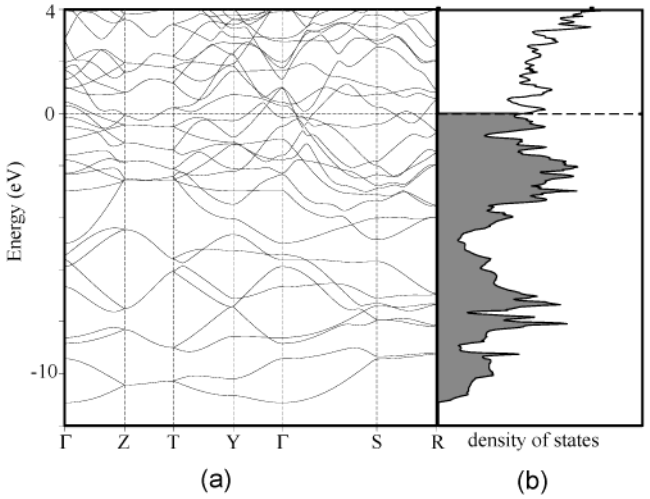

Figure 4. (a) LMTO-band structure and (b) density of states plot. The Fermi level is taken as point of zero energy.

undergoes the superconducting transition. The assumption of the demagnetization factor might be the reason of the deviation from the expected value of 100%.

A small kink in the cooling curve (arrow in Figure 3a) at 4.4 K is observed and could arise from a very small amount of a superconducting impurity. This kink is also observed during temperature-dependent measurements at fields of 20, 40, and 60 G and disappears at higher fields. Due to different transition temperatures of Sn, $SrSn_3$, and Nb_3Sn, these phases can be excluded as possible superconducting impurities. Thus another unknown superconducting phase exists in the Sr−Sn−Nb phase system.

Electronic Structure. The LMTO-band structure (Figure 4a) of $SrSn_4$ shows bands with a large dispersion crossing the Fermi level E_F revealing the metallic property. As in other superconducting binary intermetallic compounds A/AE−Sn/Pb (A = alkali metal) E_F cuts the density of states at the flank of a local maximum (Figure 4b).[13] The relatively high density of states at E_F arises from flat band sections at E_F along the symmetry lines Z−T and close to Γ at Y−Γ−S.

A topographical analysis of the electron density distribution using the electron localization function (ELF), which originally was introduced for the deduction of the shell structure of atoms from the electron density,[14] gives also insight in chemical bonding in intermetallic compounds. ELF values are scaled between 0 and 1 with the meaning that high ELF values and local ELF maxima correspond to areas and centers of localized electrons, respectively, and low ELF values define the spatial area around these maxima. The resulting partition of space into areas of high electron localization can be interpreted in terms of bonding and nonbonding electron pairs and their three-dimensional shapes. Thus spatial domains of localized electrons become visible.[15−18]

(13) Fässler, T. F. *Chem. Soc. Rev.* **2003**, *32*, 80−86.
(14) Becke, A. D.; Edgecombe, E. *J. Chem. Phys.* **1990**, *92*, 5397.
(15) Savin, A.; Becke, A. D.; Flad, J.; Nesper, R.; von Schnering, H. G. *Angew. Chem., Int. Ed. Engl.* **1997**, *36*, 2683; **1991**, *103*, 421.
(16) Silvi, B.; Savin, A. *Nature* **1994**, *371*, 683.

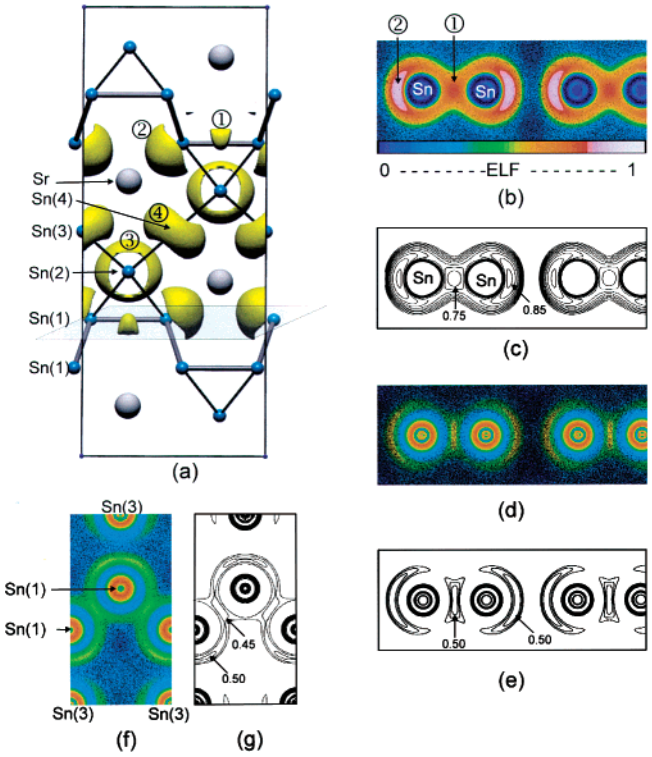

Figure 5. (a) Three-dimensional ELF representation calculated from the valence electron density. Orientation of the unit cell as in Figure 1a. The surface corresponds to the constant ELF value of 0.77. (b−e) Two-dimensional ELF represented on a cross section as indicated in Figure 6a perpendicular to the *b* direction and parallel to the Sn(1)−Sn(1) bond vector with Sn−Sn distance of 2.900 Å. (b) Density of pixels represents the valence electron density and the color of each pixel corresponds to a specific ELF value as indicated in the color bar at the bottom. (c) Contour line diagram of ELF ≤ 0.85 in line of decent steps of 0.05, and section as in Figure 6b. (d) Representation as in Figure 5b, calculated with an all electron model. (e) Contour line diagram of ELF ≤ 0.50 in line of decent steps of 0.05 of an all electron model, and section as in Figure 6c. (f, g) Two-dimensional ELF of an all-electron model represented on a cross section through the center of the Sn(1)−Sn(1) bond vector with Sn−Sn distance of 3.044 Å and parallel to the ab plane. Contour line diagram of ELF ≤ 0.50 in line of decent steps of 0.05.

The calculation has been carried out with only valence electrons or including all electrons for ELF analysis. The results are represented as a three-dimensional (3D) function of constant ELF value in Figure 5a. A two-dimensional (2D) intersection can be represented either as a pixel image (Figure 5b,d, f), where the density of pixels reflects the electron density and the color of each pixel shows the ELF value according to the color bar in Figure 5b, or as contour line diagram (Figure 5c,e,g). In the case of an all-electron calculation the shell structure of the core electrons is visible in the 2D images (Figure 5d,f). In case of the inclusion of only valence electrons deep blue areas appear at the atom site.

Figure 5a represents a 3D image of the ELF of a valence electron model. The bonding region ① corresponds to a localized bond between nearest Sn(1) atoms. This bond region is also shown in the two-dimensional intersection perpendicular to the *b* direction of the unit cell. In the color-coded representation of Figure 5b and the contour line diagram of Figure 5c the ELF maximum is located between the two Sn(1) atoms and corresponds to a covalent bond. If the ELF is calculated from the total electron density and not only from the valence electron density generally the same picture results (Figure 3d and 3e). In agreement with previous results[6] appears the bonding region ① more compressed and with lower ELF values as compared to ELF calculated from the valence electrons. The compression of the bond region is a result of repulsive interactions of ① with core electron domains (core shells). There is also a lone pair ② located at the Sn(1) atom, which points toward the Sr atom. The lone pair corresponds with respect to its direction and shape to a lone pair typically located at three-bonded atoms as e.g. the lone pair at the phosphorus atom in PF_3.[13] The bonding region between two Sn(1) atoms, which are separated by a distance of 3.044 Å (Figure 1), is visible from the two-dimensional representation parallel to the *ab* plane shown in Figure 1 and 5g. The ELF maximum of the bond region appears along the Sn(1)−Sn(1) vector. The Sn(1) atoms in Figure 1 and 5g lie above and below the intersecting plane, thus the plane shown in Figure 5f and 5g intersects the Sn(1)−Sn(1) bond. At Sn(2) a torus-type three-dimensional domain ③ is visible (Figure 5a). Distinct ELF maxima lie between the eight atom−atom connections to nearest Sn atoms (Sn(1) 4×, Sn-(3) 4×). The electron localization domain is thus of non-bonding type.[16] From the three-dimensional representation in Figure 1a it is obvious that the maximum ① is shifted slightly away from the Sn(1)−Sn(1) vector. The shift of the center of this bonding electron pair domain can be understood if we consider weak repulsive interactions with the lone-pair type region ③ of the Sn(2) atom, which lie on the opposite site with respect to the Sn(1)−Sn(1) bond vector. A similar torus-type region ④ is also observed at Sn(3), which has a quadratic-planar nearest neighbor coordination to four Sn(2) atoms. The orientation of the torus is perpendicular to the plane through neighboring Sn(2) atoms and slightly tilted in that way that the repulsion between other localization domains is minimized.

Discussion

The search for familiar structures that are related to $SrSn_4$ reveals five examples (Cr_7BC_4, $DyFe_2SiC$, $UFeS_3$, VCr_2C_2, and Rh_3Te_3) with the space group *Cmcm*, the combination of Wyckoff positions fc^2a, and the Pearson symbol oS20.[19] None of them shows a distinct structural similarity to $SrSn_4$.[19] However, if we regard $SrSn_4$ as a structure consisting of slabs of face sharing tetragonal prisms as shown in Figure 6, which alternate along b with the net of 3-fold bonded Sn(1) atoms (Figures 6a and 1c), we can trace the structure back to ones, which contain rather similar building blocks of face sharing tetragonal prisms. The structures PdBi, Mn_2AlB_2, MoAlB, and $Ru_3Al_2B_2$ contain similar slabs of face sharing tetragonal prisms. Those can further be described as intergrowth structures (IGS) of AlB_2-type and W-type slabs with a

(17) Savin, A.; Nesper, R.; Wengert, S.; Fässler, T. F. *Angew. Chem., Int. Ed. Engl.* **1997**, *36*, 2683; **1997**, *109*, 1892.
(18) Bader, R. F. W. *Coord. Chem. Rev.* **2000**, *197*, 71−94.
(19) Parthé, E.; Gelato, L. M.; Chabot, B. A.; Penzo, M.; Cenzual, K.; Gladyshevskii, R., Eds. *TYPIX-Standardized Data and Crystal Chemical Characterization of Inorganic Structure Types*; Springer-Verlag: Heidelberg, Germany, 1993; Vol. 1.

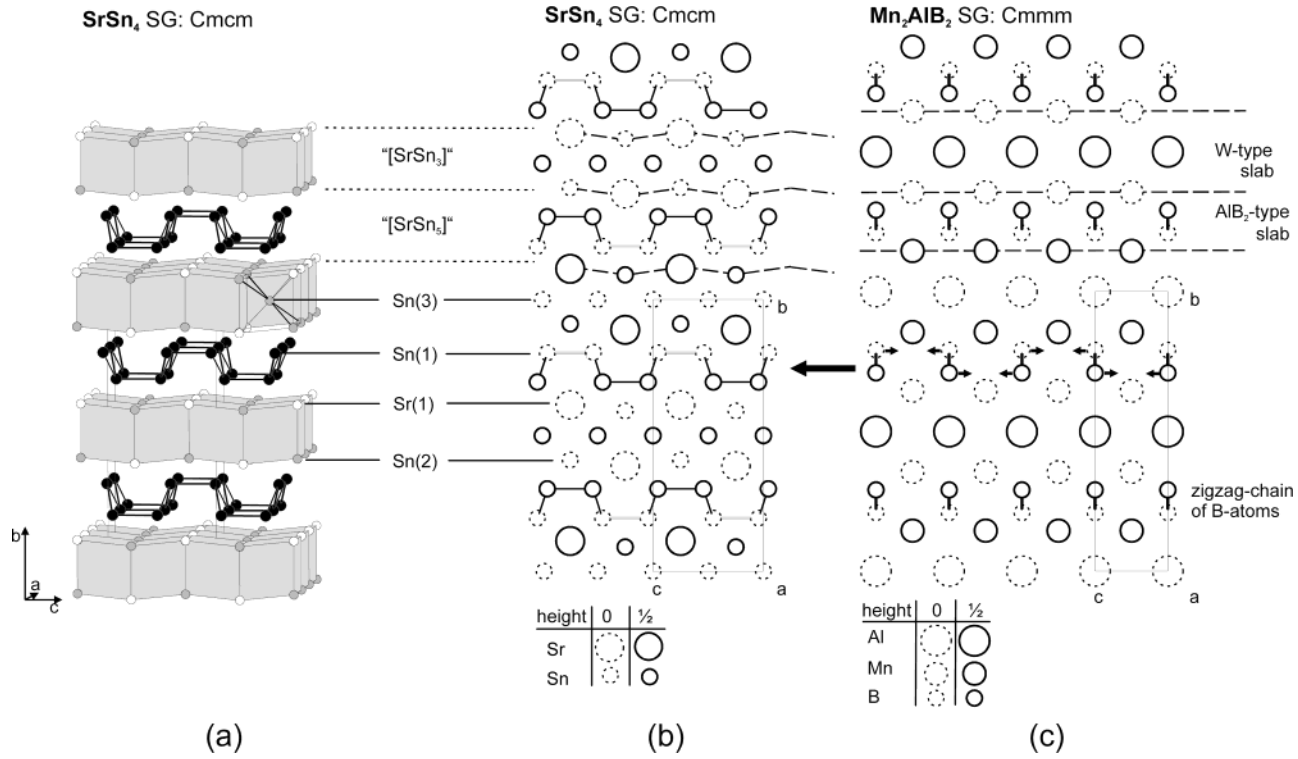

Figure 6. Structural relationship between $SrSn_4$ and Mn_2AlB_2: (a) structure of $SrSn_4$ with slabs of coordination polyhedrons of Sn(3) atoms; (b) projection of the atom sites in $SrSn_4$ along *a* with dashed lines parallel to *c* indicate the corrugation of the slab; (c) projection of Mn_2AlB_2 along *a* with highlighted slabs of AlB_2- and W-types. The heights of the atom sites along *a* are given at the bottom. See also Table 1.

variable thickness of the W-type slab.[19] Further inspection shows that Mn_2AlB_2[20] has a comparable W-type slab of three atom layers and that the AlB_2-type slab is quite similar to the observed net of Sn(1) atoms in $SrSn_4$ (Figure 1c). Both structures are shown in Figure 6b and 6c as a projection along the *a* axis. The structures are generated by two different layers of atoms: The W-type slab in Mn_2AlB_2 consists of $[AlMn_4Mn_4]$ polyhedra (Figure 6c). In $SrSn_4$ the corresponding part is build up by $[SnSn_4Sr_4]$ polyhedra, which form a slightly corrugated slab in contrast to the flat one in Mn_2AlB_2 (Figure 6a and 6b). In $SrSn_4$ the a_1/c_1 ratio of such a distorted quadratic prism (with a_1 and c_1 being prism edges along the *a* and *c* direction, respectively) is 1.31. Therefore this part of the structure can also be regarded as a part of the Cu_3Au-type slab and formal composition "$SrSn_3$" $(=Sn(3)Sn(2)_{4/8}Sr(1)_{4/8})$. The second type of slab in Mn_2AlB_2 is derived from the AlB_2 structure, if the structure is cleaved perpendicular to the planar boron atom layers in such a way that infinite B atom zigzag chain are formed. The resulting chains run parallel to the *a* axis as shown in Figure 6c. A similar slab in $SrSn_4$ can be derived from the AlB_2-type. As indicated by arrows in Figure 6c, small distortions of the B atom zigzag chains lead to the formation of a B-atom layer similar to the net of Sn(1) atoms in $SrSn_4$ (Figures 1c and 6b). Corresponding B atom layers are observed in RuB_2,[21,22] and interestingly, RuB_2 is also superconducting.[23] The formal composition of a three-dimensional structure derived from the AlB_2-type slab in $SrSn_4$ is "$SrSn_5$" $(=Sn(1)_{2/2}Sn(2)_{2/8}Sr_{2/8})$. Hence the comparison with the known compound $BaSn_5$ suggests itself. As shown earlier, the structure of $BaSn_5$ can also be rationalized as superstructure of AlB_2.[8] As a result $SrSn_4$ can be derived from one to one intergrowth structures of the composition $SrSn_3$ and $SrSn_5$.

The analysis of the structure of $SrSn_4$ using the approach of the intergrowth structure concept[24,25] offers an easy way for the representation of $SrSn_4$ although the strong conditions for the definition of slabs do not hold for this compound. The large advantage of this view is the structural relationship to compounds and a possible classification of the new structure type.

Another way of the extrusion of characteristic structural features is the analysis of the structure in terms of localized chemical bonds. At a first glance the net of Sn(1) hexagons in Figure 1c can be regarded as an analogue to the structure of neighboring group-15 elements. Considering only the shortest Sn−Sn contacts (2.900(1) and 3.044(1) Å) a net of Sn(1) atoms with exclusively three bonded (3b) atoms results. This description is an agreement with the ELF calculations, which show two types of localized bonds between Sn(1) atoms and lone pairs located at the Sn(1) atoms. Assuming that the valence electrons of strontium are exclusively transferred to these Sn(1) atoms, Sn(1) atoms are singly

(20) The structure of Mn_2AlB_2 was first described in $C222$[27] and later corrected to *Cmmm*. [28]

(21) Aronsson, B.; Stenberg, E.; Aselius, J. *Nature* **1962**, *195*, 377−378.
(22) Roof, R. B.; Kempter, C. P. *J. Chem. Phys.* **1962**, *37*, 1473−1476.
(23) Vandenberg, J. M.; Matthias, B. T.; Corenzwit, E.; Barz, H. *Mater. Res. Bull.* **1975**, *10*, 889−894.
(24) Parthé, E.; Chabot, B. A.; Cenzual, K. *Chimia* **1985**, *39*, 164−174.
(25) Grin, Y. In *Modern Perspectives in Inorganic Crystal Chemistry*; Parthé, E., Ed.; Kluwer Academic Publisher: Dordrecht, The Netherlands, Boston, MA, London, 1992; Vol. 382, pp 77−96.

negative charged and are isosteric with Sb atoms. Indeed form the Sn(1) atoms a substructure similar to those of group-15 elements (α-As type). As a consequence of singly negative charged Sn(1) atoms, the remaining Sn atoms have a formal oxidation state of zero, and in terms of the extended Zintl−Klemm−Busmann concept the formula of $SrSn_4$ is $[Sr^{2+}][(3b)Sn^{1-}]_2[Sn^0]_2$. According to the $8 - N$ rule Sn atoms with oxidation state zero should in case of exclusively covalently bound atoms be 4-fold connected. Since Sn(2) has eight and Sn(3) six surrounding Sn atoms, delocalized bonds between Sn(1) and these atoms must be assumed. This is in agreement with the distance range of 3.3−3.4 Å to neighboring Sn atoms, that are much longer than expected for localized Sn−Sn bonds. In this view Sn(2) and Sn(3) atoms must be regarded as the "metallic part" of the structure, which connects the covalently bonded nets of Sn(1) atoms. ELF mirrors this bond characteristic. There are localized bonds between Sn(1) atoms and lone pairs at these atoms. Domains of localized electrons at the "metallic" Sn(2) and Sn(3) atoms have their maxima between the atom−atom vectors. Such domains are comparable to lone pair regions in molecules and are—as shown in other cases—located energetically close to the Fermi level. Such lone pair domains are frequently present in polar intermetallic compounds, and repulsive interactions are discussed to play a crucial role for the superconductivity of these compounds.[8,13]

Comparable quadratic nets of Sn atoms are also found as building units in other binary stannides. Slightly corrugated quadratic nets of Sn atoms as shown in Figure 1b are also observed in the binary phase $NaSn_5$.[26] A framework of 4-fold bonded Sn atoms connects the coplanar two-dimensional nets. Again distances from four-connected atoms to other Sn atoms are ∼2.9 Å, whereas Sn−Sn contacts within the quadratic nets are longer (3.14 Å). In agreement with the results here, we observe localized bonds between the 4-fold connected Sn atoms in $NaSn_5$ and lone pairs at the atoms of the quadratic net. The Sn−Sn distances in $SrSn_4$ also compare well to those in $BaSn_5$, where pairs of planar hexagonal nets of Sn atoms form face-sharing hexagonal prisms, which are centered by Sn atoms. Distances from the central Sn atom to 12 atoms of the prism are 3.44 Å and are longer than the distances from the central Sn(2) atom in the distorted quadratic prism in $SrSn_4$ (3.287, 3.302 Å). Shorter distances in $SrSn_4$ are expected because of the lower coordination number of the centering atom. Sn−Sn distances along the height of the hexagonal prism in $BaSn_5$ are 2.96 Å, which compares well with the shortest contacts of 2.90 and 3.04 Å in $SrSn_4$. Short distances indicate that these are the strongest Sn−Sn interactions. The covalent character of these bonds has been revealed also for $BaSn_5$ by ELF calculations.

Summary

$SrSn_4$ represents an intermetallic compound that crystallizes in a novel structure type having covalent and metallic bond characteristics. The presence of lone pair type localization domains at the atoms of the "metallic" substructure is in coincidence with the superconducting property of $SrSn_4$. This is also observed in other intermetallic compounds.

Acknowledgment. We are grateful to the Verband der Chemischen Industrie and BMFT for support of this work. The authors thank R. Nesper, ETH Zurich, for using the SQUID magnetometer and the Siemens SMART diffractometer and B. Eisenmann, TU Darmstadt, for helpful discussions. Some of the results were presented at the Workshop on High-temperature Superconductors and Novel Inorganic Materials MSU-HTSC-VI, Moscow-St. Petersburg, June 24−30, 2001, and at the ACS conference, New Orleans, LA, March 23−27, 2003.

Supporting Information Available: Tables of data collection and refinement details, positional and thermal parameters, anisotropic displacement parameters, and important distances as well as an X-ray crystallographic file in CIF format. This material is available free of charge via the Internet at http://pubs.acs.org.

IC0302128

(26) Fässler, T. F.; Kronseder, C. *Angew. Chem., Int. Ed. Engl.* **1997**, *36*, 2683. **1998**, *110*, 1641.
(27) Becher, H. J.; Krogmann, K.; Peisker, E. *Z. Anorg. Allg. Chem.* **1966**, *344*, 140−147.
(28) Cenzual, K.; Gelato, L. M.; Penzo, M.; Parthé, E. *Acta Crystallogr.* **1991**, *B47*, 433−439.